

ADVANCED FUNCTIONAL MATERIALS



4D ELECTRONIC SYSTEMS

In article number 1903181, Yihui Zhang, John A. Rogers, and co-workers propose integrating transient materials into 3D structures, which serves as the basis for an attractive route to 4D, or transformable 3D architectures and functional electronic devices. Such devices could create opportunities for unusual applications for 3D assembly techniques, such as medical devices, microbotics, and flexible electronics.

Transformable, Freestanding 3D Mesostructures Based on Transient Materials and Mechanical Interlocking

Yoonseok Park, Haiwen Luan, Kyeongha Kwon, Shiwei Zhao, Daniel Franklin, Heling Wang, Hangbo Zhao, Wubin Bai, Jong Uk Kim, Wei Lu, Jae-Hwan Kim, Yonggang Huang, Yihui Zhang,* and John A. Rogers*

Areas of application that span almost every class of microsystems technology, from electronics to energy storage devices to chemical/biochemical sensors, can benefit from options in engineering designs that exploit 3D micro/nanostructural layouts. Recently developed methods for forming such systems exploit stress release in prestretched elastomer substrates as a driving force for the assembly of 3D functional microdevices from 2D precursors, including those that rely on the most advanced functional materials and device designs. Here, concepts that expand the options in this class of methods are introduced, to include 1) component parts built with physically transient materials to allow triggered transformation of 3D structures into other shapes and 2) mechanical interlocking elements composed of female-type lugs and male-type hooks that activate during the assembly process to irreversibly “lock-in” the 3D shapes. Wireless electronic devices demonstrate the utility of these ideas in functional systems.

Although fabrication techniques based on 3D printing,^[2,6,16–18] templated growth,^[19–21] and controlled folding/rolling^[12,22–29] are useful in many contexts, each has limitations in materials compatibility, accessible feature size or, most critically, alignment with state-of-the-art 2D processing techniques used in the semiconductor industry. A portfolio of recently presented methods allow geometric transformation of such 2D systems (referred to here as 2D precursors) into 3D structures by the action of compressive forces delivered at precisely defined locations via a prestretched silicone elastomer substrate.^[30–39] Such strategies are compatible with the most advanced planar technologies and functional materials, with feature

sizes that can span from nanometer to meter scales.^[40,41] One disadvantage is that specialized materials and techniques are required to maintain these systems in their 3D geometries after release from the elastomer substrates. This limitation is important in the context of certain fields such as microbotics.^[42–45]

1. Introduction

Complex 3D functional systems are of widespread interest due to their potential applications in areas ranging from biomedical devices^[1–7] and metamaterials^[8–11] to electronic platforms.^[12–15]

Dr. Y. Park, Dr. K. Kwon, Dr. D. Franklin, Dr. H. Zhao, Dr. W. Bai, J. U. Kim, Dr. W. Lu, J.-H. Kim
Center for Bio-Integrated Electronics
Northwestern University
Evanston, IL 60208, USA

Dr. H. Luan, S. Zhao, Dr. H. Wang
Department of Mechanical Engineering
Department of Civil and Environmental Engineering
Department of Materials Science and Engineering
Northwestern University
Evanston, IL 60208, USA

S. Zhao
School of Aeronautic Science and Engineering
Beihang University
Beijing 100191, P. R. China

J. U. Kim
School of Chemical Engineering
Sungkyunkwan University (SKKU)
Suwon 16419, Republic of Korea

J.-H. Kim
Frederick Seitz Materials Research Laboratory
Department of Materials Science and Engineering
University of Illinois at Urbana–Champaign
Urbana, IL 61801, USA

Prof. Y. Huang
Center for Bio-Integrated Electronics
Department of Mechanical Engineering
Department of Civil and Environmental Engineering
Department of Materials Science and Engineering
Northwestern University
Evanston, IL 60208, USA

Prof. Y. Zhang
Center for Flexible Electronics Technology
Applied Mechanics Laboratory
Department of Engineering Mechanics
Tsinghua University
Beijing 100084, P. R. China
E-mail: yihuizhang@tsinghua.edu.cn

Prof. J. A. Rogers
Department of Materials Science and Engineering
Biomedical Engineering, Neurological Surgery, Chemistry, Mechanical Engineering, Electrical Engineering and Computer Science Simpson Querrey Institute and Feinberg Medical School
Center for Bio-Integrated Electronics
Northwestern University Evanston
Evanston, IL 60208, USA
E-mail: jrogers@northwestern.edu

 The ORCID identification number(s) for the author(s) of this article can be found under <https://doi.org/10.1002/adfm.201903181>.

DOI: 10.1002/adfm.201903181

where published approaches to free-standing 3D structures based on shape memory polymers (SMPs)^[31] and plastic deformation^[21,46] might constrain design and/or processing options. An additional drawback is that beyond certain changes that can be realized by deforming the elastomer substrate, the 3D geometries are fixed. The combined use of ideas for forming free-standing structures in 4D forms, i.e., geometries/functions that can transform with time, could be important in many contexts, particularly those in implantable/ingestible biomedical devices, bioelectronics systems, and active tissue scaffolds.^[8,47–50]

Here, we introduce a set of strategies that address these two challenges. 1) 4D structures: The idea for 4D assembly relies on the combination of 2D layers of physically transient materials (e.g., poly(lactic-co-glycolic acid) (PLGA) and silicon membranes) with those that are nontransient (e.g., polyimide (PI), metal, photodefinable epoxy). Exposing the resulting 3D structures to conditions (e.g., immersion in phosphate-buffered saline (PBS) solution at a pH of 7.4) that trigger a transient process leads a change in 3D shape and/or function over time, as a form of 4D assembly. 2) Freestanding 3D structures: The idea for freestanding structures exploits interlocking designs that consist of female-type lugs and male-type hooks. As a 2D precursor with such structures geometrically transforms by release of prestrain in the substrate, aligned hooks and lugs engage and mechanically interlock in a manner that fixes the 3D shape. Dissolution of sacrificial layers on the substrate yields stable, freestanding forms. Demonstrations of these concepts focus on freestanding, transformable 3D electronic systems, in the form of wireless, battery-free light emitting devices. These approaches create opportunities for unusual applications of 3D assembly techniques in medical devices, microbotics, flexible electronics, and many others.

2. Results and Discussion

2.1. Transformable 3D Structure by Transient Materials

Figure 1A presents a schematic exploded view illustration of a multilayer 2D precursor that includes layers of PLGA (10 μm) and Cu coated PI (Cu, 50 nm/PI, 10 μm) with lithographically defined bonding sites on a prestretched elastomer ($\epsilon_{\text{app1}} = 70\%$). Layers of PLGA (5 μm) above and below the Cu/PI layer ensure

sufficient adhesion between these materials. The Cu/PI layer then forms a 3D structure upon compressive buckling due to forces imparted through the bonding sites (Figure S1 and S2, Supporting Information). Details appear in the Experimental Section. Dissolving the PLGA by immersion in PBS (70 $^{\circ}\text{C}$, pH 7.4) leads to geometrical transformation into a distinct 3D architecture, as shown in Figure 1B and finite element analysis (FEA) models capture the change in height and internal strain in 3D structure over 10 days (Figure S3, Supporting Information). The strain in the PLGA increases from around 1% to 2.5% during the first 7 days and dramatically to 9% on the 8th day, with total dissolution on the 10th day. The strain in the Cu/PI layer decreases through this same time period. The height of the 3D structure remains ≈ 1.0 mm for 9 days and ultimately rises to 3 mm. Optical images captured at day 0, 3, and 10 highlight these changes. The initially transparent PLGA layer turns opaque by day 3 due to hydrolytic degradation, swelling, and microcracking. The PLGA loses its mechanical strength via random chemical scission of the ester backbone and within 10 days, full dissolution occurs. The 3D structure transforms into an intermediate state as mechanical constraints associated with PLGA layer decrease by its partial degradation. After complete dissolution at day 10, the 3D structure reaches its final geometry, corresponding to a structure that incorporates only nontransient materials. Complete elimination of the residual PLGA requires more than 10 days, as determined by the chemical composition and molecular weight.^[51,52]

Figure 2A presents a collection of experimental results and FEA predictions for various designs using bi- and uni-axially prestretched elastomer substrates. In these cases, the PLGA imposes a transient mechanical constraint on the coated ribbons/membranes, such that the shape transforms upon dissolution of the PLGA. The heights of the 3D structures depend on the lengths of the 2D precursors and the magnitudes of the prestrain. The PLGA mechanically joins ribbons with different lengths such that they buckle together. Upon dissolution, this coupling vanishes, leading to physically disconnected ribbon/membrane components that move to yield a distinct 3D configuration. 3D structures constructed by uniaxial compressive buckling undergo similar but comparatively simple changes. The middle section of the 3D structures in the experiment is curved due to residual stresses that arise during fabrication, which are not included in the FEA result. Figure 2B shows the

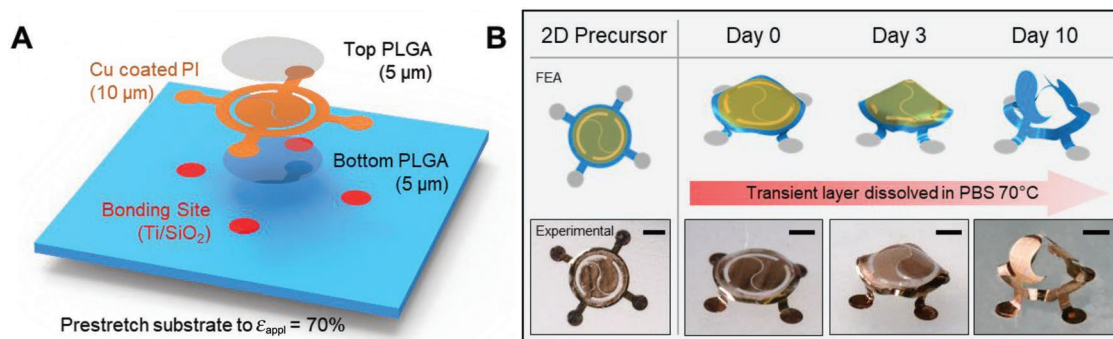


Figure 1. Transformable 3D mesostructures enabled by transient components. A) Schematic exploded view illustration of a 2D precursor that consists of film of patterned layers of PI (coated with Cu) and PLGA, to highlight the layout. B) Demonstration shape transformation of a corresponding 3D structure formed from this 2D precursor by mechanical assembly by dissolution of the PLGA via immersion in PBS at 70 $^{\circ}\text{C}$. Scale bar 1 mm.

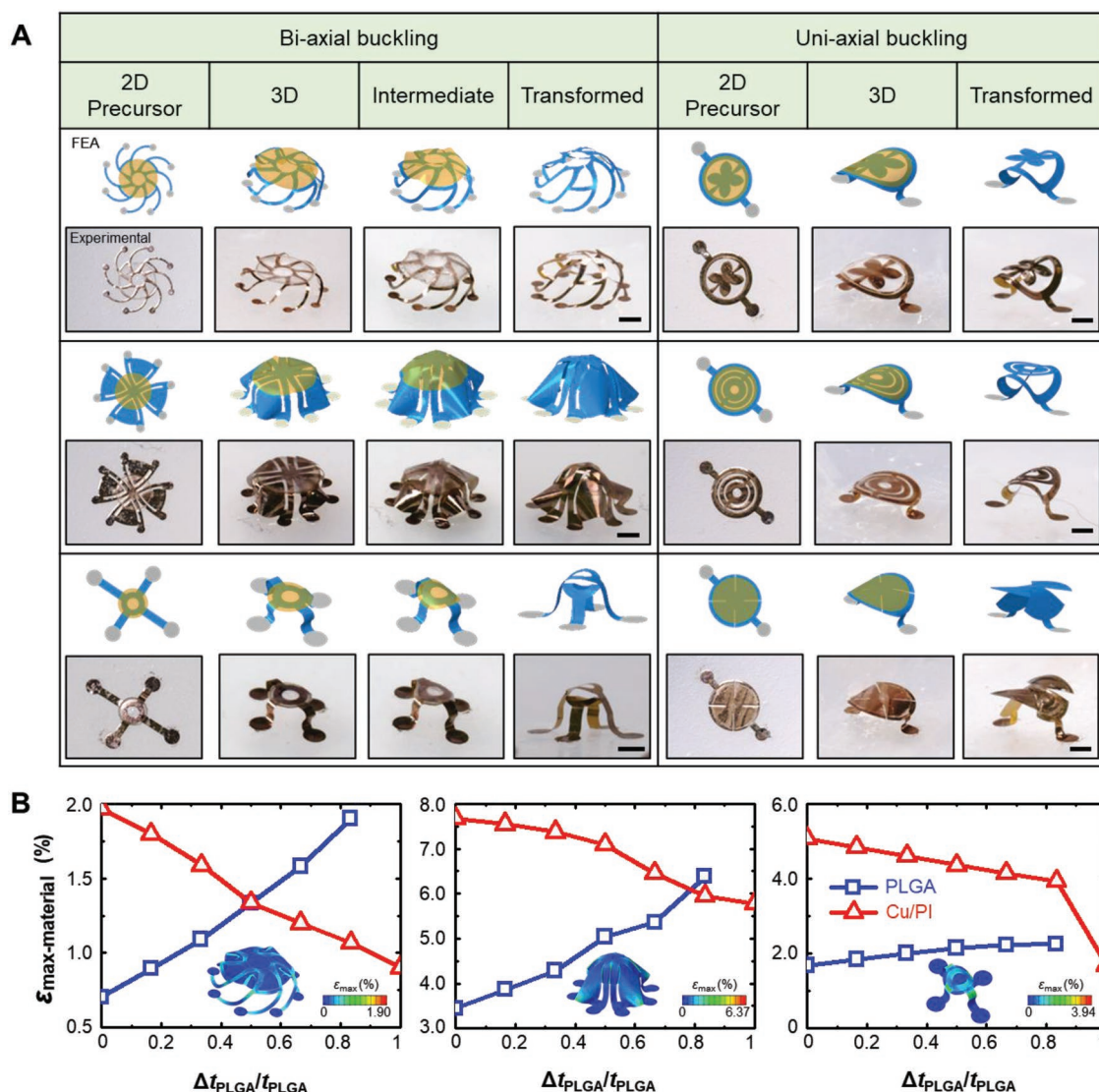


Figure 2. Assorted collection of transformable 3D mesostructures. A) Experimental images and FEA predictions of transformable 3D structures formed by bi-/uni-axial compressive buckling. Scale bar 1 mm. B) Dependence of the maximum principal strain in the Cu/PI and in PLGA components of these structures on the thickness of the PLGA.

evolution of the maximum principal strain in the Cu/PI and PLGA during the dissolution of the latter, corresponding to a gradual reduction in thickness, assumed to occur uniformly in FEA modeling. The gradual dissolution of the PLGA layer increases and decreases the material strain in the PLGA and Cu/PI, respectively. The model considers only a change in the thickness of the PLGA to account for its degradation, specifically a linear decrease day 0 to day 10 (with the total dissolution on day 10).^[53] For the three designs shown in Figure 2A (left), the maximum principal strains ($\epsilon_{\max\text{-material}}$) increase in the PLGA and decrease in the Cu/PI, throughout the process of dissolution. **Figure 3** presents coherently coupled multilayered 3D structures, uniquely enabled by the transient layers, and microscale transformable 3D structures using photodefined epoxy (SU8) and Si (1.5 μm in thickness) membranes.

Figure 3A presents FEA results and optical images of 3D mesostructures with entangled topologies. Here, a

micromanipulation process yields interweaving elements in the 2D precursor. In this design, the PLGA layer (blue) lies above the Cu/PI layer (orange) at the contacting points i, ii, and iv and below at the point ii. These entangled transient and nontransient ribbons form a 3D mesostructure that resembles a twisted knot. Dissolution of the PLGA transforms the interwoven 3D structure into a nonwoven one. Figure 3B shows an image of an entangled 3D structure that uses layers of PLGA above and below a bilayer 2D ribbon structure. Dissolution of the PLGA yields a nonwoven 3D structure.

Transient materials not only provide access to geometrically transformable 3D structures, but also create opportunities in 3D structures that are uniquely realizable in this way, as shown in Figure 3C. In this case, 2D precursors without transient layers consist of two separate parts that remain on the substrate surface during release of the prestrain. The addition of a joining layer of PLGA leads to assembly into a 3D mesostructure.

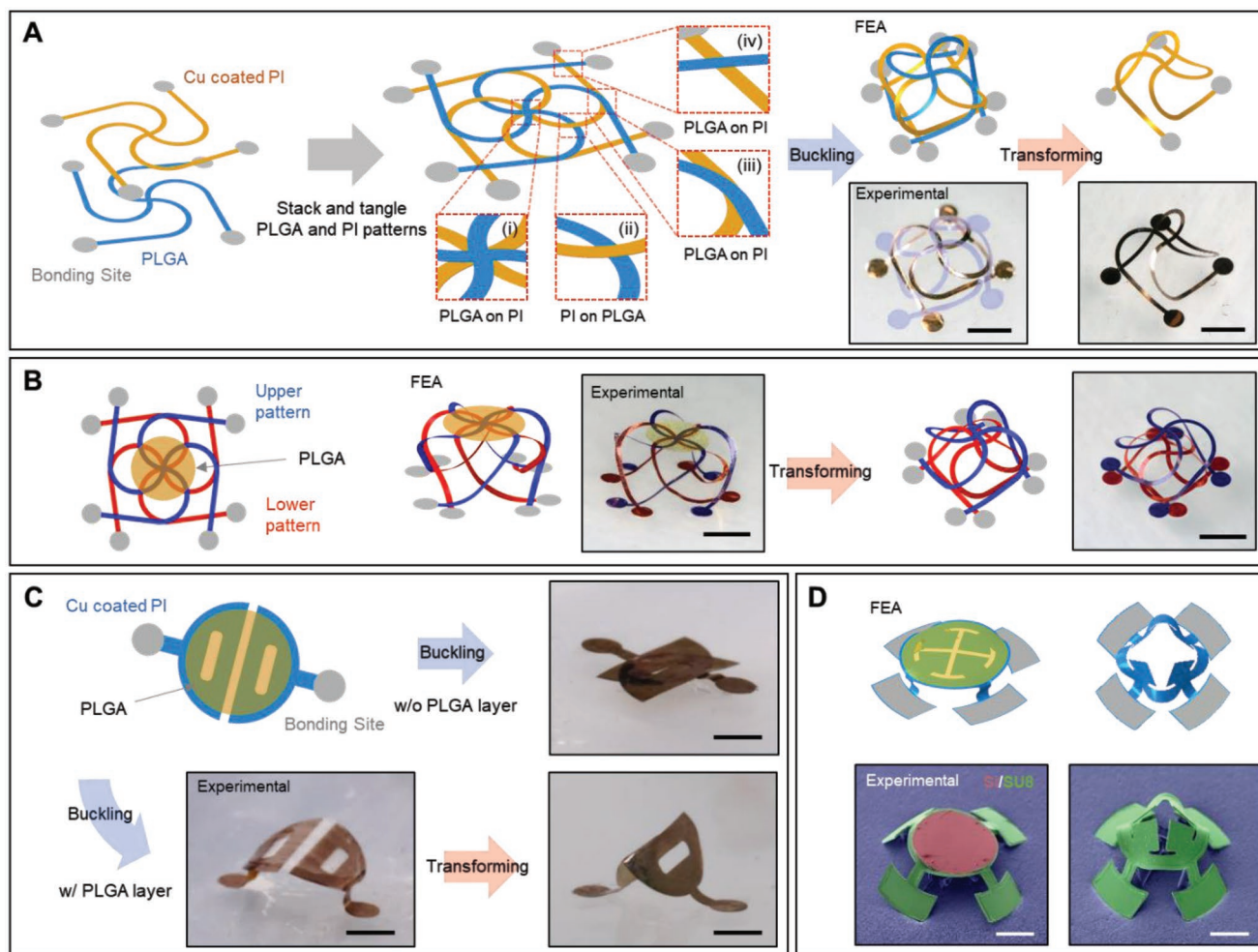


Figure 3. Transformable 3D mesostructures based on diverse geometries, including entangled topologies, and various transient materials. A) Schematic illustration of the procedures for fabricating 2D precursors for 3D interwoven multilayer structures of Cu/PI and PLGA bilayers and transformation from an interwoven 3D buckling structure to a monolayer 3D structure. B) Interwoven-like 2D precursor and 3D structure using a transient layer of PLGA. C) 2D precursors consist of two separated parts with a joining layer of PLGA. This structure releases from the substrate to form a 3D structure. By comparison, otherwise similar 2D precursors without the PLGA remain on the substrate. Upon dissolution of the PLGA, the two Cu/PI parts lean against one another to form an unusual 3D mesostructure that would be difficult or impossible to create directly, with out transient PLGA component. D) FEA predictions and experimental images (optical) of a microstructure constructed with Si/SU8. Dissolving the Si by immersion in PBS (70 °C) transforms the 3D microstructure into another shape. Scale bar 1 mm, for structures in A–C and 100 μm for D.

Upon dissolution of the PLGA, the two remaining parts lean against one another to hold an unusual 3D shape as predicted by FEA modeling (Figure S4, Supporting Information).

The processes described above can be implemented in microscale structures, as shown in the example of Figure 3D. The constituent parts here include a photodefined layer of epoxy (SU8, Microchem, 7 μm in thickness) and a transient layer of monocrystalline silicon (1.5 μm in thickness). The dissolution rate for Si is 140 nm d^{-1} in PBS at 67 °C,^[52,54] such that full dissolution occurs within 10 days, leading to a geometry transformation that is consistent with FEA modeling.

2.2. Freestanding 3D Structures by Mechanical Interlocking

A mechanical interlocking strategy provides a route to the irreversible assembly of 3D structures that hold their shapes,

independent of forces imparted to them by the substrate. 3D structures, transformed by linear elastic mechanics due to compressive forces, transform back into their original geometry when released from elastomer substrate. The examples presented here use hook-shaped male parts and lug-shaped female parts located at each bonding site across each 2D precursor. When a hook inserts into a lug during assembly, the two parts mechanically interlock to fix the shape of the corresponding 3D structure. **Figure 4A** shows optical images and FEA results of the process. The scheme begins with the transfer of the 2D precursor structure, with an underlying sacrificial layer, onto a pre-stretched ($\epsilon_{\text{appl-x}} = \epsilon_{\text{appl-y}} = 70\%$) elastomer substrate. **Figure 4B** shows the controlled path and interlocking mechanism of the female and male parts in the interlocking system. Release of the stretched elastomer follows the sequence: Initial state ($\epsilon_{\text{appl-x}} = 70\%$) \rightarrow State I ($\epsilon_{\text{appl-x}} = 35\%$) \rightarrow State II ($\epsilon_{\text{appl-x}} = 0\%$). At the intermediate State I, the lug-shaped female part forms

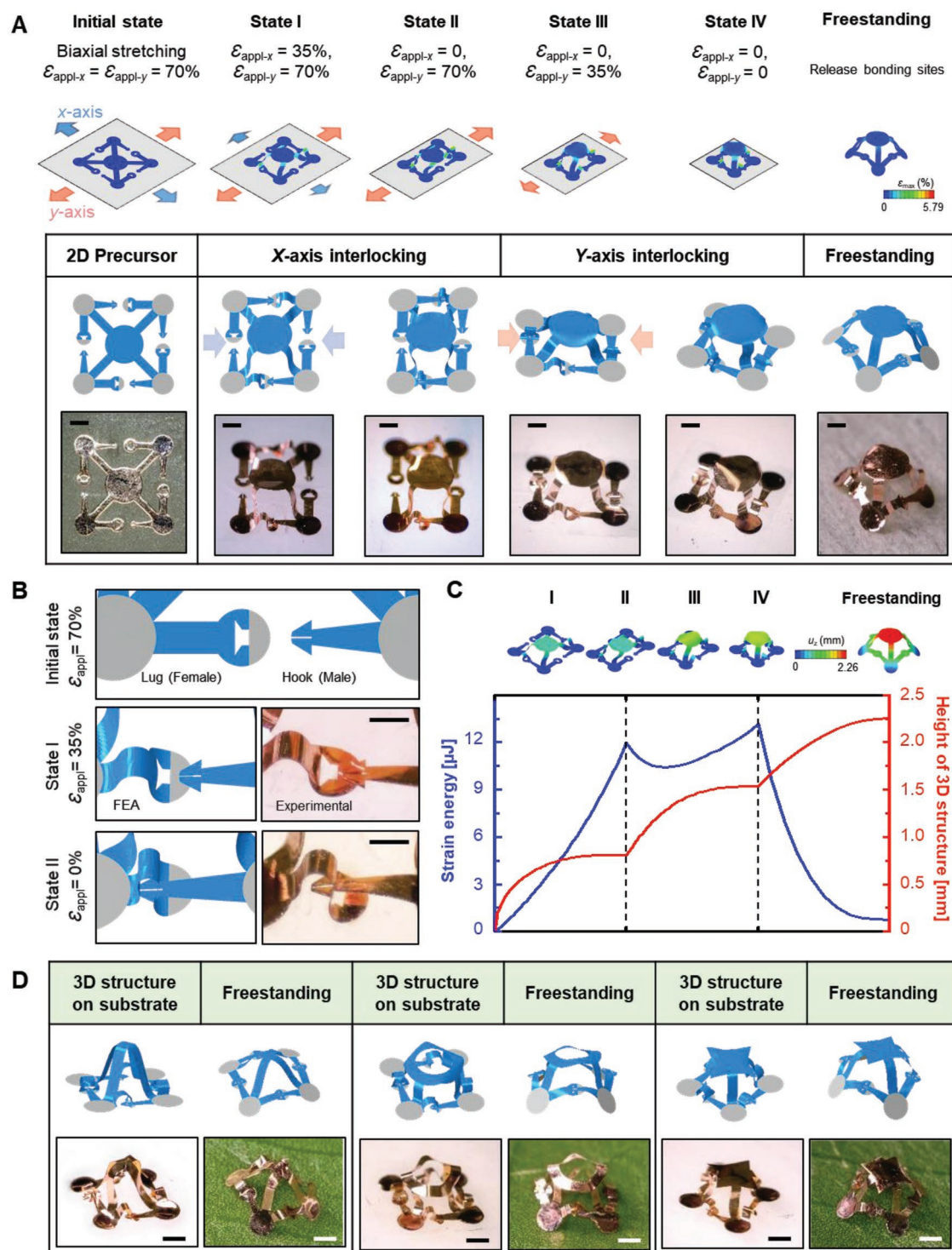


Figure 4. Freestanding 3D mesostructures that use a mechanical interlocking system. A) Conceptual illustration of the fabrication process through a sequence of FEA results and experimental images (optical) for a representative 3D structure. 1) selective bonding of a 2D precursor onto a substrate prestretched to 70% biaxial strain; 2) releasing the X-axis strain to 35%, thereby producing 3D openings in which hooks can be mechanically interlocked; 3) releasing the X-axis strain to 0%, thereby interlocking the hooks and lugs; 4) releasing the Y-axis strain to 35% and 0%, thereby completing the interlocking of the whole system; 5) dissolving the sacrificial layer (Mg) at the bonding sites, thereby releasing the 3D structure from substrate. B) FEA results and photographs of the interlocking process at the initial stage and at states I and II. C) Evolution of strain energy and height of the 3D interlocking system from 2D configuration to X-direction interlocking, to Y-direction interlocking, and finally to the freestanding state. D) FEA predictions and experimental images of various 3D mesostructures on a substrate and transferred onto a leaf after release. Scale bars 1 mm for structures in A and D, 500 μm for structure in B.

a 3D open space and the end of the hook from an associated bonding site reaches to the gate of opening. Full release of the prestrain along the X-axis produces State II, wherein the hook inserts into the lug and engages mechanical interlocking. After connecting the hooks and lugs along the X-axis, interlocking along Y-axis follows in sequence: State III ($\epsilon_{\text{appl-y}} = 35\%$) \rightarrow State IV ($\epsilon_{\text{appl-y}} = 0\%$), such that all four sets of hooks and lugs are mechanically joined. A customized equal-biaxial stretching stage controls the amount of stretching at each state (Figure S5, Supporting Information) and FEA models captured the behaviors in a quantitative fashion. The process can follow an X- to Y-axis sequence or the reverse. Figure 4C shows that the strain energy in the 3D structure increases during the X-direction interlocking (ended as State II), and decreases until a local minimum is reached, after which it increases again to a slightly higher level (the peak value) during the subsequent Y-direction interlocking (ended as State IV). The decrease between State II and State IV can be attributed to the release of local deformations/strains that occur at the joints near bonding sites during initiation of the Y-direction interlocking. After releasing the bonding sites of the mechanically interlocked 3D structure, the interlocking of hook and lug serves as a bonding site to hold 3D structure in freestanding form and the strain energy in the freestanding system decreases drastically to $\approx 10\%$ of the peak value. The height of the 3D structure increases sequentially during the entire processes of 3D assembly, interlocking, and bonding releasing (Figure 4C). The unfolding and rotation near the bonding sites contribute to most of this increase during the bonding release process. A thin film of magnesium (Mg, 200 nm in thickness, Figure S6, Supporting Information) serves as a sacrificial layer at the bonding sites to allow release from the substrates upon immersion in water.^[31] Figure 4D shows various freestanding 3D structures by FEA and optical images. Assembly of an array (4 by 4, 24 pairs of hooks and lugs, Figure S7, Supporting Information) of 3D structures shows high yields in mechanical interlocking.

2.3. 4D Electronic Systems

4D systems, as defined by 3D structures that can alter their geometries in space and time, may find utility in areas such as biomedical engineering, as ingestible microbots and tissue grippers.^[22,55–57] Systems of this type that incorporate electronic components (e.g., light emitting diodes (LEDs), photodiode, near filed communication antenna, capacitor) can provide various potential therapeutic and diagnostic capabilities inside the body. As an illustration, Figure 5 shows an exploded-view diagram of the 2D layout of a wirelessly powered lighting system with a coating of parylene-C (Figure S8, Supporting Information) as an encapsulant. Dissolution of the transient PLGA cladding layer follows from immersion in PBS solution (70 °C and pH 7.4) for 10 days, thereby initiating the geometric transformation (Figure S9, Supporting Information). The electronics show no change in performance during this period. Specifically, energy harvesting occurs through coupling to a 13.56 MHz external loop antenna with high quality factor (Figure 5D). The Cu receiver coil (18 μm in thickness, line width/spacing 100/60 μm , outer diameter 6 mm and 7 turns) connects in parallel with a 39 pF capacitor,

to offer high performance, matching operation at this frequency. This wireless coupling activates the LEDs when the device is placed in the near-field of the transmission antenna. Transformation slight shifts the resonance frequency of the Cu coil from 13.56 to 13.70 MHz but dramatically changes the angular output characteristics of the LEDs (Figure 5E). Specifically, the LEDs are tilted 9.6° (Figure S10, Supporting Information) and the divergence of light distribution increases as shown in Figure 4D, with possible utility in light therapy approaches that might benefit from automatic changes in illumination profiles over time.

3. Conclusion

In summary, integrating transient materials into 3D structures serves as the basis of an attractive route to 4D, or transformable, 3D architectures and functional electronic devices across length scale from micrometers to centimeters. Mechanical interlocking systems provide straightforward access to freestanding 3D structures, without limitation in materials selection. Demonstrations described here include a diversity of transformable and freestanding 3D meso- and microstructures based on these concepts. The integration of electronic components and transient layers into 2D precursor yields freestanding 4D functional devices, as illustrated in wirelessly powered LEDs integrated 4D electronics. The addition of these ideas to other previously reported concepts in 3D assembly expands the range of design possibilities, with potential uses in transformable and/or freestanding optoelectronics, biomedical, communication, and energy storage devices. Extension to multistaged transformation by selective transience and to structures with dimensions smaller than those reported here represent topics of current work.

4. Experimental Section

Fabrication of Transformable 3D PLGA/Cu/PI Mesostructures: Preparation of 2D precursors began with spin coating (3000 rpm for 30 s) and curing (180 °C for 2 min) a thin layer of poly(methylmethacrylate) (PMMA) onto a clean glass slide, followed by spin coating and fully curing (260 °C for 1 h) a layer of polyimide (10 μm ; PI-2545, HD MicroSystems). A thin film of copper (Cu, 50 nm) deposited on the PI by sputtering and patterned by photolithography and wet etching served as a hard mask for oxygen plasma etching (220 mT, 200 W, 30 min) of the PI. Immersion in acetone overnight dissolved the underlying PMMA layer, thereby allowing the structures to be retrieved from the glass slide. PLGA layers (5 μm) were prepared by slowly drying a solution of this material on a hydrophobic surface (e.g., Si substrate with a self-assembled monolayer formed using trimethoxymethylsilane). Patterning of these layers used a laser cutting system. Stamps of poly (dimethylsiloxane) (PDMS) enabled delivery of the patterned PLGA onto the surface of a water-soluble tape (polyvinyl alcohol; PVA 3M Co.). A similar transfer process delivered the Cu/PI 2D precursor to the PLGA/PVA and, subsequently, another patterned layer of PLGA onto the resulting multilayer assembly, i.e., Cu/PI precursor/PLGA/PVA. Annealing at 50 °C under a vapor of ethyl acetate bonded the top and bottom layers of PLGA. Deposition of Ti/SiO₂ (10 nm/50 nm in thickness) via electron beam evaporation through a shadow mask onto the back sides of the structures defined the bonding sites. Exposing the 2D precursors and the elastomer surface to ultraviolet (UV)-ozone generated surface hydroxyl groups to facilitate bonding. Pre-stretching the elastomer to an equal biaxial strain of 70%, laminating the 2D precursors/PVA tape onto the stretched elastomer and heating (70 °C for 10 min) led to strong bonding with a thin (≈ 0.7 mm) sheet of

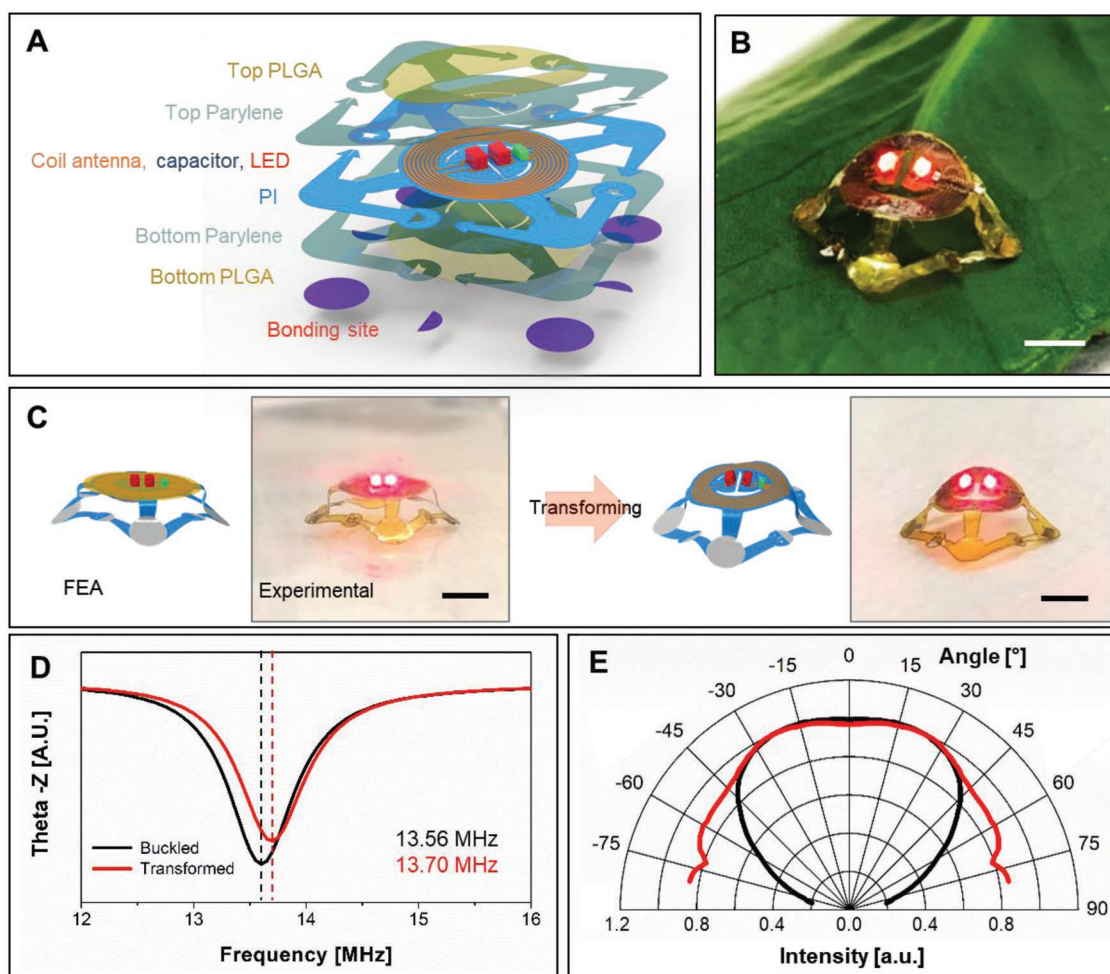


Figure 5. Transformable, freestanding 3D electronic wireless systems. A) Schematic exploded view illustration of the multilayer 2D precursor, including the PI support, transient PLGA layers, Parylene-C encapsulation layers, coil antenna, capacitor, and LEDs. B) Freestanding 3D electronic system resting on a leaf. Wireless power transmission (WPT) capability visualized by activating the LED by placing the 3D structures inside an external loop antenna. C) FEA predictions, experimental images, and angular dependence of the emission of LEDs in 3D electronic systems before and after immersion in PBS solution at 70 °C for 10 days. D) Impedance phase plot as a function of frequency for the near-field WPT antenna, showing the quality factor of the Cu coil in the buckled and transformed system. E) Angular dependent emission intensity as buckled and transformed. Scale bar 3 mm.

silicone elastomer (Dragon Skin, Smooth-On). Dissolving the PVA tape with water and releasing the prestrain transformed the 2D precursors into 3D forms.

Fabrication of Transformable 3D Silicon/Epoxy Mesostructures: Preparation of the 2D precursors began with patterning the top silicon layer (1.5 μm in thickness) on a silicon-on-insulator (SOI) wafer by photolithography and dry etching, followed by spin coating (3000 rpm for 30 s) and baking of an adhesive layer (Omni-coat). Spin coating (7 μm in thickness; 3000 rpm for 40 s) and lithographically patterning a photo definable epoxy (SU8, Microchem) created a supporting layer for the silicon. Oxygen plasma etching (190 mT, 100 W, 1 min) removed the exposed adhesive layer. Briefly (90 s) immersing the sample in hydrofluoric acid (HF, 49%) partially undercut the SiO_2 layer. Another photolithography step using AZ 5214 on top of the SU8 layer defined the bonding sites. Immersion in HF (49%) for 4 h fully undercut the SiO_2 . Electron beam evaporation of Ti/ SiO_2 (10 nm/50 nm in thickness) through a shadow mask defined bonding sites. The remaining steps (transfer printing, buckling) were similar to the procedures described above. Immersing the 2D precursor in acetone removed the AZ 5214 prior to buckling.

Fabrication of Freestanding 3D Mesostructures: Preparation of 2D precursors (patterning except PLGA bonding) followed steps similar to

those described above. Electron beam evaporation of Ti/Mg/Ti/ SiO_2 (10/200/10 nm/50 nm in thickness) through a shadow mask formed bonding sites. Releasing a prestrained elastomer along the X-axis and Y-axis independently led to interlocking of the female type lugs and male type hooks, thereby fixing the 3D structures and allowing their detachment from the elastomer. Immersion in water overnight dissolved the Mg to release the 3D structures into freestanding forms.

Fabrication of 4D Electronics: Preparation of 2D precursors began with laminating a film of Cu (18 μm thickness) on a slab of PDMS (10:1, Sylgard 184), followed by defining a Cu coil antenna by laser cutting (LPKF4 UV laser system). Lamination delivered a film of PI (12 μm in thickness; Kapton, Fralock) onto a glass slide coated with a layer of cured PDMS (3000 rpm) as a temporary adhesive layer. A partially cured (60 °C for 60 s) film of PI (2 μm in thickness; PI-2545, HD MicroSystems) was then spin cast (3000 rpm for 30 s) on the laminated PI film. Pressing the Cu coil against the half-cured PI film led to bonding during a process of complete curing in a vacuum oven (260 °C for 1 h). LEDs (LX0402S1C, peak wavelength 636 nm, Lumex Opto/Components Inc) and capacitors were mounted at selectively defined locations on the 2D Cu precursor with conductive epoxy (Allied Electronics Corp., Fort Worth, TX). A coating of parylene (14 μm thickness) formed by chemical

vapor deposition served as an encapsulation layer. The remaining steps (PLGA bonding, buckling and releasing) were similar to the procedures described above.

Finite Element Analysis of Mechanically Guided Buckling: Computational models of post-buckling analyses utilized the commercial finite element analysis software (Abaqus) to predict the 3D configurations. Eight-node solid elements (C3D8R) and four-node shell elements (S4R) were chosen for the elastomer substrate and 2D precursors, respectively. Convergence of mesh sizes was tested to ensure computational accuracy. In the simulations, the Mooney–Rivlin strain energy potential model was chosen for elastomer substrates with hyperelastic material behavior. The substrate material was modeled as incompressible, with an elastic modulus of 166 kPa. Polyimide, SU8, PLGA, SU8, parylene C and silicon (Si) are modeled with a linear elastic behavior, with the elastic modulus and Poisson's ratio given by $E_{PI} = 2.5$ GPa and $\nu_{PI} = 0.34$ for PI; $E_{PLGA} = 1.37$ GPa and $\nu_{PLGA} = 0.44$ for PLGA; $E_{SU8} = 4.02$ GPa and $\nu_{SU8} = 0.22$ for SU8; $E_{parylene} = 2.76$ GPa and $\nu_{parylene} = 0.4$ for parylene C; and $E_{Si} = 130$ GPa and $\nu_{Si} = 0.27$ for silicon. Metals such as copper were assumed to follow an elastoplastic constitutive relationship. An idealized elastoplastic model (without hardening) was used in simulations, and the yield strain was chosen as 0.3%. The elastic modulus (E) and Poisson's ratio (ν) are $E_{Cu} = 119$ GPa and $\nu_{Cu} = 0.34$ for copper (Cu).

Angular Dependent Intensity Measurement: Light emission from the LED-integrated structures was characterized using a home-built goniometer setup. Samples and an RF power source were mounted on a micropositioner stage assembly to provide XYZ and rotational control. A fiber (QP400-1-UV-VIS, Ocean Optics) with collimating optics (74-UV, Ocean Optics) placed adjacent to the mounted sample captured light and passed this light to a spectrometer (Flame-S-VIS-NIR-ES, Ocean Optics). The stage position was then calibrated to find the eucentric point and to determine relative intensity of the LED system as a function of rotational position.

Supporting Information

Supporting Information is available from the Wiley Online Library or from the author.

Acknowledgements

Y.P. and H.L. contributed equally to this work. The team acknowledges support from NSF (CMMI 1635443). Y.P. acknowledges the support from German Research Foundation (PA 3154/1-1). Y.Z. acknowledges the support from the National Natural Science Foundation of China (11672152 and 11722217) and the Tsinghua National Laboratory for Information Science and Technology. Y.H. acknowledges the support from the NSF (CMMI1400169 and CMMI1534120). This work utilized Northwestern University Micro/Nano Fabrication Facility (NUFAB), which is partially supported by Soft and Hybrid Nanotechnology Experimental (SHyNE) Resource (NSF ECCS-1542205), the Materials Research Science and Engineering Center (DMR-1720139), the State of Illinois, and Northwestern University. Typographical errors within the main text and affiliations were corrected on October 4th, 2019 after initial online publication.

Conflict of Interest

The authors declare no conflict of interest.

Keywords

3D mesostructure, 4D structure, freestanding, microelectronics, transformable

Received: April 20, 2019
Revised: June 27, 2019
Published online: July 26, 2019

- [1] X. Dai, W. Zhou, T. Gao, J. Liu, C. M. Lieber, *Nat. Nanotechnol.* **2016**, *11*, 776.
- [2] X. Liu, H. Yuk, S. Lin, G. A. Parada, T.-C. Tang, E. Tham, C. de la Fuente-Nunez, T. K. Lu, X. Zhao, *Adv. Mater.* **2018**, *30*, 1704821.
- [3] B. Tian, J. Liu, T. Dvir, L. Jin, J. H. Tsui, Q. Qing, Z. Suo, R. Langer, D. S. Kohane, C. M. Lieber, *Nat. Mater.* **2012**, *11*, 986.
- [4] R. Feiner, L. Engel, S. Fleischer, M. Malki, I. Gal, A. Shapira, Y. Shacham-Diamand, T. Dvir, *Nat. Mater.* **2016**, *15*, 679.
- [5] T. G. Leong, C. L. Randall, B. R. Benson, N. Bassik, G. M. Stern, D. H. Gracias, *Proc. Natl. Acad. Sci. USA* **2009**, *106*, 703.
- [6] M. S. Mannoor, Z. Jiang, T. James, Y. L. Kong, K. A. Malatesta, W. O. Soboyejo, N. Verma, D. H. Gracias, M. C. McAlpine, *Nano Lett.* **2013**, *13*, 2634.
- [7] G. Rijal, W. Li, *Sci. Adv.* **2017**, *3*, e1700764.
- [8] G. Liu, Y. Zhao, G. Wu, J. Lu, *Sci. Adv.* **2018**, *4*, eaat0641.
- [9] S. Zhao, Y. Li, H. Yin, Z. Liu, E. Luan, F. Zhao, Z. Tang, S. Liu, *Sci. Adv.* **2015**, *1*, e1500372.
- [10] S. Chisca, V.-E. Musteata, R. Sougrat, A. R. Behzad, S. P. Nunes, *Sci. Adv.* **2018**, *4*, eaat0713.
- [11] Y. Tang, G. Lin, S. Yang, Y. K. Yi, R. D. Kamien, J. Yin, *Adv. Mater.* **2017**, *29*, 1604262.
- [12] D. Grimm, C. C. Bof Bufon, C. Deneke, P. Atkinson, D. J. Thurmer, F. Schäffel, S. Gorantla, A. Bachmatiuk, O. G. Schmidt, *Nano Lett.* **2013**, *13*, 213.
- [13] J.-H. Ahn, H.-S. Kim, K. J. Lee, S. Jeon, S. J. Kang, Y. Sun, R. G. Nuzzo, J. A. Rogers, J. A. Rogers, J. A. Lewis, *Science* **2006**, *314*, 1754.
- [14] W. Liu, Z. Chen, G. Zhou, Y. Sun, H. R. Lee, C. Liu, H. Yao, Z. Bao, Y. Cui, *Adv. Mater.* **2016**, *28*, 3578.
- [15] K. Dong, J. Deng, Y. Zi, Y.-C. Wang, C. Xu, H. Zou, W. Ding, Y. Dai, B. Gu, B. Sun, Z. L. Wang, *Adv. Mater.* **2017**, *29*, 1702648.
- [16] D. B. Kolesky, R. L. Truby, A. S. Gladman, T. A. Busbee, K. A. Homan, J. A. Lewis, *Adv. Mater.* **2014**, *26*, 3124.
- [17] A. Cangialosi, C. Yoon, J. Liu, Q. Huang, J. Guo, T. D. Nguyen, D. H. Gracias, R. Schulman, *Science* **2017**, *357*, 1126.
- [18] L. C. Hsiao, A. Z. M. Badruddoza, L.-C. Cheng, P. S. Doyle, *Soft Matter* **2017**, *13*, 921.
- [19] S. Noda, K. Tomoda, N. Yamamoto, A. Chutinan, *Science* **2000**, *289*, 604.
- [20] S. Y. Lin, J. G. Fleming, D. L. Hetherington, B. K. Smith, R. Biswas, K. M. Ho, M. M. Sigalas, W. Zubrzycki, S. R. Kurtz, J. Bur, *Nature* **1998**, *394*, 251.
- [21] Z. Yan, M. Han, Y. Shi, A. Badea, Y. Yang, A. Kulkarni, E. Hanson, M. E. Kandel, X. Wen, F. Zhang, Y. Luo, Q. Lin, H. Zhang, X. Guo, Y. Huang, K. Nan, S. Jia, A. W. Orham, M. B. Mevis, J. Lim, X. Guo, M. Gao, W. Ryu, K. J. Yu, B. G. Nicolau, A. Petronico, S. S. Rubakhin, J. Lou, P. M. Ajayan, K. Thornton, G. Popescu, D. Fang, J. V. Sweedler, P. V. Braun, H. Zhang, R. G. Nuzzo, Y. Huang, Y. Zhang, J. A. Rogers, *Proc. Natl. Acad. Sci. USA* **2017**, *114*, E9455.
- [22] W. Xu, Z. Qin, C.-T. Chen, H. R. Kwag, Q. Ma, A. Sarkar, M. J. Buehler, D. H. Gracias, *Sci. Adv.* **2017**, *3*, e1701084.
- [23] Y. Xia, G. Cedillo-Servin, R. D. Kamien, S. Yang, *Adv. Mater.* **2016**, *28*, 9637.
- [24] E. Hawkes, B. An, N. M. Benbernou, H. Tanaka, S. Kim, E. D. Demaine, D. Rus, R. J. Wood, *Proc. Natl. Acad. Sci. USA* **2010**, *107*, 12441.
- [25] C. Py, P. Reverdy, L. Doppler, J. Bico, B. Roman, C. N. Baroud, *Phys. Rev. Lett.* **2007**, *98*, 156103.
- [26] S. Xu, Z. Yan, K.-I. Jang, W. Huang, H. Fu, J. Kim, Z. Wei, M. Flavin, J. McCracken, R. Wang, A. Badea, Y. Liu, D. Xiao, G. Zhou, J. Lee, H. U. Chung, H. Cheng, W. Ren, A. Banks, X. Li, U. Paik, R. G. Nuzzo, Y. Huang, Y. Zhang, J. A. Rogers, *Science* **2015**, *347*, 154.

- [27] Y. Mei, A. A. Solovov, S. Sanchez, O. G. Schmidt, *Chem. Soc. Rev.* **2011**, *40*, 2109.
- [28] C. Xu, X. Wu, G. Huang, Y. Mei, *Adv. Mater. Technol.* **2018**, *4*, 1800486.
- [29] R. Streubel, J. Lee, D. Makarov, M.-Y. Im, D. Karnaushenko, L. Han, R. Schäfer, P. Fischer, S.-K. Kim, O. G. Schmidt, *Adv. Mater.* **2014**, *26*, 316.
- [30] J. Rogers, Y. Huang, O. G. Schmidt, D. H. Gracias, *MRS Bull.* **2016**, *41*, 123.
- [31] X. Wang, X. Guo, J. Ye, N. Zheng, P. Kohli, D. Choi, Y. Zhang, Z. Xie, Q. Zhang, H. Luan, K. Nan, B. H. Kim, Y. Xu, X. Shan, W. Bai, R. Sun, Z. Wang, H. Jang, F. Zhang, Y. Ma, Z. Xu, X. Feng, T. Xie, Y. Huang, Y. Zhang, J. A. Rogers, *Adv. Mater.* **2019**, *31*, 1805615.
- [32] Z. Yan, F. Zhang, J. Wang, F. Liu, X. Guo, K. Nan, Q. Lin, M. Gao, D. Xiao, Y. Shi, Y. Qiu, H. Luan, J. H. Kim, Y. Wang, H. Luo, M. Han, Y. Huang, Y. Zhang, J. A. Rogers, *Adv. Funct. Mater.* **2016**, *26*, 2629.
- [33] K.-I. Jang, K. Li, H. U. Chung, S. Xu, H. N. Jung, Y. Yang, J. W. Kwak, H. H. Jung, J. Song, C. Yang, A. Wang, Z. Liu, J. Y. Lee, B. H. Kim, J.-H. Kim, J. Lee, Y. Yu, B. J. Kim, H. Jang, K. J. Yu, J. Kim, J. W. Lee, J.-W. Jeong, Y. M. Song, Y. Huang, Y. Zhang, J. A. Rogers, *Nat. Commun.* **2017**, *8*, 15894.
- [34] B. H. Kim, F. Liu, Y. Yu, H. Jang, Z. Xie, K. Li, J. Lee, J. Y. Jeong, A. Ryu, Y. Lee, D. H. Kim, X. Wang, K. Lee, J. Y. Lee, S. M. Won, N. Oh, J. Kim, J. Y. Kim, S.-J. Jeong, K.-I. Jang, S. Lee, Y. Huang, Y. Zhang, J. A. Rogers, *Adv. Funct. Mater.* **2018**, *28*, 1803149.
- [35] M. Han, H. Wang, Y. Yang, C. Liang, W. Bai, Z. Yan, H. Li, Y. Xue, X. Wang, B. Akar, H. Zhao, H. Luan, J. Lim, I. Kandela, G. A. Ameer, Y. Zhang, Y. Huang, J. A. Rogers, *Nat. Electron.* **2019**, *2*, 26.
- [36] Z. Yan, F. Zhang, F. Liu, M. Han, D. Ou, Y. Liu, Q. Lin, X. Guo, H. Fu, Z. Xie, M. Gao, Y. Huang, J. Kim, Y. Qiu, K. Nan, J. Kim, P. Gutruf, H. Luo, A. Zhao, K.-C. Hwang, Y. Huang, Y. Zhang, J. A. Rogers, *Sci. Adv.* **2016**, *2*, e1601014.
- [37] M. Humood, Y. Shi, M. Han, J. Lefebvre, Z. Yan, M. Pharr, Y. Zhang, Y. Huang, J. A. Rogers, A. A. Polycarpou, *Small* **2018**, *14*, 1703852.
- [38] X. Ning, X. Yu, H. Wang, R. Sun, R. E. Corman, H. Li, C. M. Lee, Y. Xue, A. Chempakasseril, Y. Yao, Z. Zhang, H. Luan, Z. Wang, W. Xia, X. Feng, R. H. Ewoldt, Y. Huang, Y. Zhang, J. A. Rogers, *Sci. Adv.* **2018**, *4*, eaat8313.
- [39] H. Zhao, K. Li, M. Han, F. Zhu, A. Vázquez-Guardado, P. Guo, Z. Xie, Y. Park, L. Chen, X. Wang, H. Luan, Y. Yang, H. Wang, C. Liang, Y. Xue, R. D. Schaller, D. Chanda, Y. Huang, Y. Zhang, J. A. Rogers, *Proc. Natl. Acad. Sci. USA* **2019**, *116*, 201901193.
- [40] Y. Zhang, Z. Yan, K. Nan, D. Xiao, Y. Liu, H. Luan, H. Fu, X. Wang, Q. Yang, J. Wang, W. Ren, H. Si, F. Liu, L. Yang, H. Li, J. Wang, X. Guo, H. Luo, L. Wang, Y. Huang, J. A. Rogers, *Proc. Natl. Acad. Sci. USA* **2015**, *112*, 11757.
- [41] Y. Zhang, F. Zhang, Z. Yan, Q. Ma, X. Li, Y. Huang, J. A. Rogers, *Nat. Rev. Mater.* **2017**, *2*, 17019.
- [42] Y. Alapan, O. Yasa, O. Schauer, J. Giltinan, A. F. Tabak, V. Sourjik, M. Sitti, *Sci. Rob.* **2018**, *3*, eaar4423.
- [43] M. A. Zeeshan, R. Grisch, E. Pellicer, K. M. Sivaraman, K. E. Peyer, J. Sort, B. Özkale, M. S. Sakar, B. J. Nelson, S. Pané, *Small* **2014**, *10*, 1284.
- [44] M. Sitti, *Nature* **2009**, *458*, 1121.
- [45] M. Medina-Sánchez, V. Magdanz, M. Guix, V. M. Fomin, O. G. Schmidt, *Adv. Funct. Mater.* **2018**, *28*, 1707228.
- [46] Y. Shi, F. Zhang, K. Nan, X. Wang, J. Wang, Y. Zhang, Y. Zhang, H. Luan, K.-C. Hwang, Y. Huang, J. A. Rogers, Y. Zhang, *Extreme Mech. Lett.* **2017**, *11*, 105.
- [47] Z. Ding, C. Yuan, X. Peng, T. Wang, H. J. Qi, M. L. Dunn, *Sci. Adv.* **2017**, *3*, e1602890.
- [48] C. Yang, M. Boorugu, A. Dopp, J. Ren, R. Martin, D. Han, W. Choi, H. Lee, *Mater. Horiz.* **2019**, *6*, 1244.
- [49] A. Sydney Gladman, E. A. Matsumoto, R. G. Nuzzo, L. Mahadevan, J. A. Lewis, *Nat. Mater.* **2016**, *15*, 413.
- [50] C. de Marco, S. Pané, B. J. Nelson, *Sci. Rob.* **2018**, *3*, eaau0449.
- [51] A. Göpferich, *Biomaterials* **1996**, *17*, 103.
- [52] J.-K. Chang, H. Fang, C. A. Bower, E. Song, X. Yu, J. A. Rogers, *Proc. Natl. Acad. Sci. USA* **2017**, *114*, E5522.
- [53] R. Li, H. Cheng, Y. Su, S.-W. Hwang, L. Yin, H. Tao, M. A. Brenckle, D.-H. Kim, F. G. Omenetto, J. A. Rogers, Y. Huang, *Adv. Funct. Mater.* **2013**, *23*, 3106.
- [54] L. Yin, A. B. Farimani, K. Min, N. Vishal, J. Lam, Y. K. Lee, N. R. Aluru, J. A. Rogers, *Adv. Mater.* **2015**, *27*, 1857.
- [55] H. Fu, K. Nan, W. Bai, W. Huang, K. Bai, L. Lu, C. Zhou, Y. Liu, F. Liu, J. Wang, M. Han, Z. Yan, H. Luan, Y. Zhang, Y. Zhang, J. Zhao, X. Cheng, M. Li, J. W. Lee, Y. Liu, D. Fang, X. Li, Y. Huang, Y. Zhang, J. A. Rogers, *Nat. Mater.* **2018**, *17*, 268.
- [56] B. G. Compton, J. A. Lewis, *Adv. Mater.* **2014**, *26*, 5930.
- [57] K. Malachowski, M. Jamal, Q. Jin, B. Polat, C. J. Morris, D. H. Gracias, *Nano Lett.* **2014**, *14*, 4164.